Available online at www.sciencedirect.com
SCIENCE DIRECT
Applied Catalysis B: Environmental 66 (2006) 81–91
APPLIED CATALYSIS B: ENVIRONMENTAL
www.elsevier.com/locate/apcatb

Probing the factors affecting structure and activity of the Au/CeO_2 system in total and preferential oxidation of CO

Francesco Arena [a,b,*], Pio Famulari [a], Giuseppe Trunfio [a], Giuseppe Bonura [b], Francesco Frusteri [b], Lorenzo Spadaro [b]

[a] *Dipartimento di Chimica Industriale e Ingegneria dei Materiali, Università degli Studi di Messina, Salita Sperone 31, I-98166 S. Agata (Messina), Italy*
[b] *Istituto CNR-ITAE "Nicola Giordano", Salita S. Lucia 39, I-98126 S. Lucia (Messina), Italy*

Received 16 December 2005; received in revised form 17 February 2006; accepted 21 February 2006
Available online 2 May 2006

Abstract

The effects of the preparation method (deposition–precipitation, co-precipitation, incipient-wetness, combustion) and loading (1–5 wt.%) on the structure and redox features of the Au/CeO_2 system have been probed by XRD, TEM and TPR techniques. The catalytic pattern in total (TOX) and preferential (PROX) CO oxidation has been assessed by temperature programmed reaction tests in the range 273–473 K. Controlling surface area and residual chlorine, the synthesis route determines the strength of the $Au–CeO_2$ interaction which, reflecting in a hard reduction of the active phase, hinders the CO oxidation functionality. Chlorine removal by *washing treatment* in diluted alkaline solutions enables an easy reduction of the active phase, levelling off the TOX and PROX performance of the various systems.

Keywords: Au/CeO_2 catalyst; Preparation method; Reduction pattern; Surface area; Chlorine; Dispersion; Total and preferential CO oxidation

1. Introduction

For long time regarded as a catalytically inactive material because of its chemical "inertness" towards almost all elements and compounds [1], last decades have witnessed a rapid growth of research interest on Au catalysts [2–29] as, contrarily to the bulk metal, supported systems drive effectively various reactions such as NO_x reduction, oxidative dehydrogenation, hydrochlorination, epoxidation [2–14]. Moreover, Au catalysts exhibit a superior performance in *total* (TOX) and *preferential* (PROX) CO oxidation and water-gas-shift reactions [2,4–9,15–29], showing higher activity, stability and resistance to moisture than other noble-metal systems.

The stabilisation of Au clusters with an average diameter of 2–3 nm on suitable oxide supports is essential for attaining active catalysts, as *nanosized* particles do not exhibit the conventional *noble* behaviour denoting, instead, a peculiar reactivity towards oxygen, hydrogen, water and carbon monoxide molecules, due to some specific active centres at the Au/support interface [2–9,15–17,22–29].

Deposition–precipitation, *co-precipitation* and *phosphine grafting* are recommended synthesis routes, whereas conventional impregnation methods (incipient wetness, electrostatic adsorption, etc.) generally lead to poorly active systems [2–7,20,25,28].

Also support plays a crucial role as reducible oxides, mostly Fe_2O_3 and TiO_2, confer a higher reactivity to Au catalysts [2,4–7,19]. However, both basic (MgO, $Be(OH)_2$) and refractory (SiO_2, Al_2O_3, ZrO_2, etc.) oxides can also allow to attain very active catalysts [4–7,10–16,20,28]. In particular, providing fairly active oxygen species, reducible oxide supports could mask the *particle size effect* in the CO oxidation [2–7,19].

Despite of the extensive research work on catalyst design and characterisation, yet, the exact nature of active sites is still controversial and reaction mechanisms involving either Au atoms and/or ions are still under debate [2–7,12–29].

Although a peculiar redox activity of the ceria support confers a unique reactivity to supported catalysts [30], only few reports have been till now devoted to the physico-chemical and catalytic features of the Au/CeO_2 system [21–24,29]. Bera and Hegdè studied the reactivity of a 1% Au/CeO_2 catalyst obtained

* Corresponding author. Tel.: +39 090 6765606; fax: +39 090 391518.
E-mail address: Francesco.Arena@unime.it (F. Arena).

0926-3373/$ – see front matter © 2006 Elsevier B.V. All rights reserved.
doi:10.1016/j.apcatb.2006.02.023

by the combustion route in the SCR of NO and total oxidation of CH_4 and CO, stressing a beneficial effect of a high temperature (1073 K) calcination treatment on activity, due to an improved metal dispersion [21]. However, it has been recently documented that a ''microcrystalline'' ceria support (SA_{BET}, 180 m^2/g) enhances the activity of Au by two orders of magnitude, yielding also a full carbon dioxide selectivity in the PROX reaction [29]. Previously, Fu et al. ascribed a very high activity of ''*nanostructured*'' Au/CeO_2 catalysts in the LT-WGS reaction to an enhanced reducibility [22,23], while Tabakova et al. emphasised the effects of synthesis on Au dispersion and LT-WGS activity [24].

Therefore, this study is aimed at assessing the effects of the preparation method and Au loading on total and preferential CO oxidation activity of the Au/CeO_2 system. Basic relationships amongst chemical, structure, redox and catalytic properties of the various systems are discussed.

2. Experimental

2.1. Materials

The studied catalysts were prepared by deposition–precipitation (DP), incipient-wetness (IW), co-precipitation under ultrasound irradiation (CP) and combustion (CB) routes, according to the following experimental procedures.

2.1.1. Deposition–precipitation (DP)

A 1% Au/CeO_2 catalyst (DP(1)) was prepared by deposition–precipitation under stirring of the $HAuCl_4{\cdot}3H_2O$ (*Carlo Erba*, >99%) precursor on a powdered ceria sample (SA_{BET}, 44 m^2/g) obtained by the combustion route (see *infra*). The pH of the suspension was progressively raised by drop-wise addition of a 0.1 M Na_2CO_3 solution until a final value of ca. 9. After ageing, the solid was filtered, washed with hot distilled water and then dried at 373 K (16 h).

2.1.2. Incipient-wetness (IW)

A 1% Au/CeO_2 catalyst (IW(1)) was prepared by incipient-wetness of the above ceria sample with an aqueous solution ($\approx$8 mL/g_{cat}) of the $HAuCl_4$ precursor (pH $\approx$ 2). After impregnation, the catalyst was dried at 373 K (16 h).

2.1.3. Co-precipitation (CP)

A 1% Au/CeO_2 catalyst (CP(1)) was prepared by co-precipitation of the $HAuCl_4$ and $(NH_4)_2Ce(NO_3)_6{\cdot}9H_2O$ (*Fluka*, >99%) precursors in aqueous solution at r.t. under ultrasound irradiation [31], by adding a 5 wt.% Na_2CO_3 solution until a pH value of ca. 9. After precipitation, the solid was ''aged'' at r.t., then filtered and washed with hot distilled water and further dried at 373 K (16 h).

2.1.4. Combustion (CB)

Differently loaded (1–5 wt.%) Au/CeO_2 catalysts (CB(x)) were prepared by the combustion route, following the procedure indicated by Bera and Hegdè [21]. Aqueous solutions of $(NH_4)_2Ce(NO_3)_6$, $HAuCl_4$ and urea (*fuel*) were mixed in a borosilicate dish, and then introduced into a muffle furnace preheated at 673 K. After water evaporation, the mixture ignited with a cold-flame, leaving a *sponge*-like solid.

All the catalysts (''*untreated*'') were studied without any further treatment, unless otherwise specified.

The list of the catalysts along with relative notation, Au loading (as evaluated by XRF analysis), SA_{BET} values and residual chlorine, is presented in Table 1.

3. Methods

Washing treatment and quantitative analysis of residual chlorine were carried out by dispersing ca. 3 g of catalyst samples into a 50 ml NaOH aqueous solution (pH $\approx$ 9) at 333 K under stirring. The resulting solution of three extractions ($\approx$150 ml) was used for quantitative analysis of chloride by the *Volhard method*, while the catalyst sample was further washed with distilled water and dried again at 373 K (16 h).

TEM characterisation of Au/CeO_2 catalysts was performed by a *Philips CM12* Transmission Electron Microscope (resolution, 0.2 nm). Powdered samples were dispersed in isopropanol under ultrasound irradiation and the resulting suspension put drop-wise on a standard copper grid coated with a porous carbon film.

X-ray diffraction (*XRD*) patterns of the catalysts were obtained by an APD-2000 diffractometer (*Ital-Structures*) operated at 40 kV and 30 mA, employing the Ni-filtered Cu Kα radiation (λ = 1.5406 Å). Identification of XRD patterns was made on the basis of the JCPDS database [32], while the particle size of gold and ceria was determined by the Scherrer's equation assuming a Gaussian shape of the peaks.

Temperature programmed reduction (*TPR*) measurements were performed in a linear quartz micro-reactor (id, 4 mm) fed with a 6% H_2/Ar purified carrier at the rate of 60 STP ml min^{-1}. The experiments were carried out in the range 293–1073 K with

Table 1
List of the studied catalysts

Code	Preparation method	Au loading (wt.%)	SA_{BET} (m^2/g)	[Cl] (wt.%)	Cl_{at}/Au_{at}
CeO_2	Combustion	–	44	–	–
CB(1)	Combustion	0.85	30	0.27	1.9
CB(3)	Combustion	3.00	24	0.79	1.8
CB(5)	Combustion	4.90	27	n.d.	–
DP(1)	Deposition–precipitation	1.00	35	–	0.0
CP(1)	Co-precipitation	0.95	150	–	0.0
IW(1)	Incipient-wetness	1.00	50	0.68	3.8

a heating rate of 12 K min^{-1}, keeping constant (ca. 1 mg) the Au load. The hydrogen consumption was monitored by a TCD, calibrated by the peak area of known amounts of CuO. TPR data resulted very reproducible both in maximum position (±3 K) and extent of H_2 consumption (±3%).

Catalyst testing in the CO oxidation reaction, in absence (TOX) and presence of hydrogen (PROX), were performed by temperature programmed reaction tests, using a linear quartz reactor (id, 4 mm) connected to a quadrupole mass spectrometer (*Thermolab*, *Fisons Instruments*) by a heated (453 K) inlet capillary system (transit time <0.5 s). All the tests were run in the range 273–473 K with a heating rate of 4 K min^{-1}, using 0.02 g of catalyst diluted with 0.1 g of powder SiC. CO/O_2/He and CO/O_2/H_2/He reaction mixtures in the molar ratios 2/2/96 and 1/2/50/47 flowing at 50 and 100 STP ml min^{-1} were used for TOX and PROX tests, respectively. Using the SEM amplifier (1200 V), mass spectra were recorded in *multiple ion monitoring* mode, acquiring the signals relative to the following mass-to-charge (*m*/*z*) ratios: 2 (H_2), 4 (He), 44 (CO_2), 28 (CO), 17 (OH), and 32 (O_2). With helium as internal standard, CO and H_2 conversion at any temperature was derived from CO/He and H_2/He signals ratio, respectively:

$$X_{CO} = 1 - \frac{(P_{CO}/P_{He})_T}{(P_{CO}/P_{He})_{273\,K}}, \qquad X_{H_2} = 1 - \frac{(P_{H_2}/P_{He})_T}{(P_{H_2}/P_{He})_{273\,K}}$$

Further, for mass-balance calculation, the response factor ($f_x = [I \quad R]^{-1}$) of OH and CO_2 were determined from the relative sensitivity factor (*R*) of the *m*/*z* ratios 17 and 44 with respect to 28 (CO) and the cracking pattern (i.e., the abundance of the considered fragment (*m*/*z*) in the mass spectrum, *I*) of H_2O and CO_2. Conversion values from the mass balance:

$$X_Y = \frac{P_X/f_X}{P_X/f_X + P_Y/f_Y}$$

where Y and X stand for reactant and the corresponding product, respectively, were in a satisfactory agreement (±10%) with those obtained by the internal standard method. The kinetic constant values from the *pseudo-first order* integral equation were used for Arrhenius plot correlations of CO and H_2 oxidation, considering always conversion values below 25%.

4. Results

4.1. Redox behaviour

The TPR patterns in the range 293–1073 K of the CeO_2 support and Au/CeO_2 catalysts, obtained by different synthesis routes, are shown in Fig. 1, while the onset temperature of reduction ($T_{o,red}$), the temperature of peak maximum (T_{Mi}) and the H_2 consumption, expressed both as total number of moles (273–1073 K) and number of H_2 molecules consumed *per* Au atom (273–623 K), are summarised in Table 2.

The TPR pattern of the ceria matrix features a main peak centred at ca. 700 K with a shoulder on the high-*T* side,

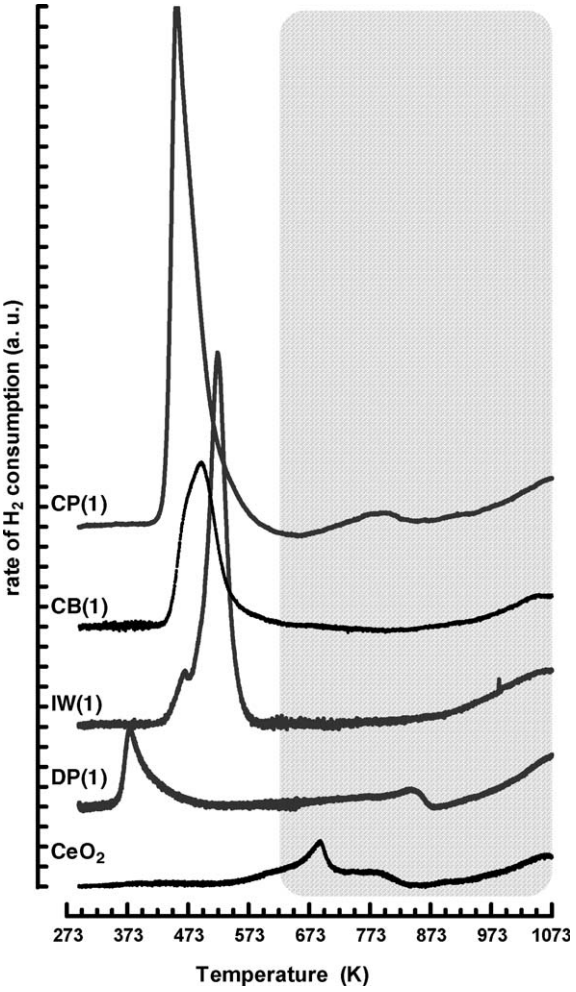

Fig. 1. TPR profiles of the "untreated" YY(1) catalysts. *Effect of the preparation method* (the dashed grey area includes the temperature range for reduction of the ceria support).

attributable to the reduction of surface/sub-surface Ce^{4+} ions with a different degree of coordinative unsaturation. Coupled to the baseline drift between 873 and 1073 K, prompted by the ongoing reduction of Ce^{4+} ions in the bulk [22,23,30], the hydrogen consumption equals 637 μmol/g accounting for a reduction degree of ca. 22%.

Table 2
TPR data of "untreated" Au/CeO_2 catalysts (effects of preparation method and loading)

Sample	$T_{o,red}$ (K)	T_{M1} (K)	T_{M2} (K)	H_2 consumption	
				μmol/g_{cat} [a]	H_2/Au [b]
CeO_2	504	692	–	637	–
DP(1)	345	376	–	812	6.1
CP(1)	402	455	–	2603	43.1
IW(1)	423	522	–	1836	23.9
CB(1)	421	495	1052	1173	21.3
CB(3)	401	473	1021	741	2.8
CB(5)	399	473	–	727	1.5

[a] Relative to the range 273–1073 K.
[b] Relative to the range 273–623 K.

Quite dissimilar from that of the ceria support, the TPR profile of the Au/CeO_2 catalysts consists of one peak, whose position, shape and intensity depend on the synthesis route.

The DP(1) catalyst features the easiest reducibility, evidenced by the lowest $T_{o,red}$ (340 K) and T_{M1} (376 K) values, along with the "lowest" H_2 consumption, corresponding to a H_2/Au ratio equal to 6.1, anyhow quite larger than the stoichiometric consumption (1.5) for reduction of the Au precursor. With the highest $T_{o,red}$ (423 K) and T_{M1} (522 K) values, the IW(1) is the least reducible catalyst, while a much larger intensity of the main peak accounts for a H_2/Au value equal to 23.9. The CB(1) sample displays a "broader" reduction peak with a similar $T_{o,red}$ (421 K), but centred at lower T (T_{M1}, 495 K), whose intensity corresponds to a H_2/Au ratio of 21.9. Characterised by a much larger total surface area (Table 1), the CP(1) sample features the biggest reduction peak, with intermediate onset ($T_{o,red}$, 401 K) and centre (T_{M1}, 455 K) positions, which accounts for the largest H_2/Au ratio (43.1).

Moreover, at $T > 723$ K all the catalysts feature a slight rate of H_2 consumption which still denotes the incipient reduction of the underlying support in the bulk.

The effect of the Au loading on the TPR pattern of combustion catalysts (CB(x)) are shown in Fig. 2, while numeric data are included in Table 2. A gold content in the range 0.85–4.9 wt.% does not affect the spectral features described for the CB(1) sample, and consisting of a main peak with maximum centred between 473 and 522 K and a zone of low H_2 consumption rate at $T > 673$ K. Rising the loading, the peak becomes narrower and more symmetric (Fig. 2) and its maximum shifts to lower T (Table 2), while the H_2/Au ratio decreases sharply from 21.3 (CB(1)) to 1.5 (CB(5)).

On the whole, the above data indicate that development of total surface area (A) and Au precursor dispersion (B) are the key-issues linked to preparation method and loading, respec-

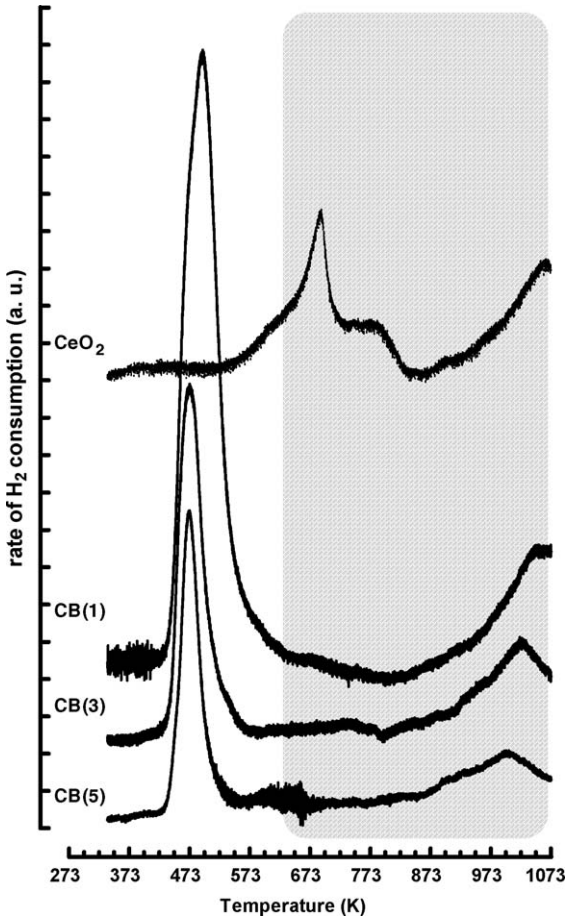

Fig. 2. TPR profiles of the "untreated" CB(x) catalysts. *Effect of the Au loading* (the dashed grey area includes the temperature range for reduction of the ceria support).

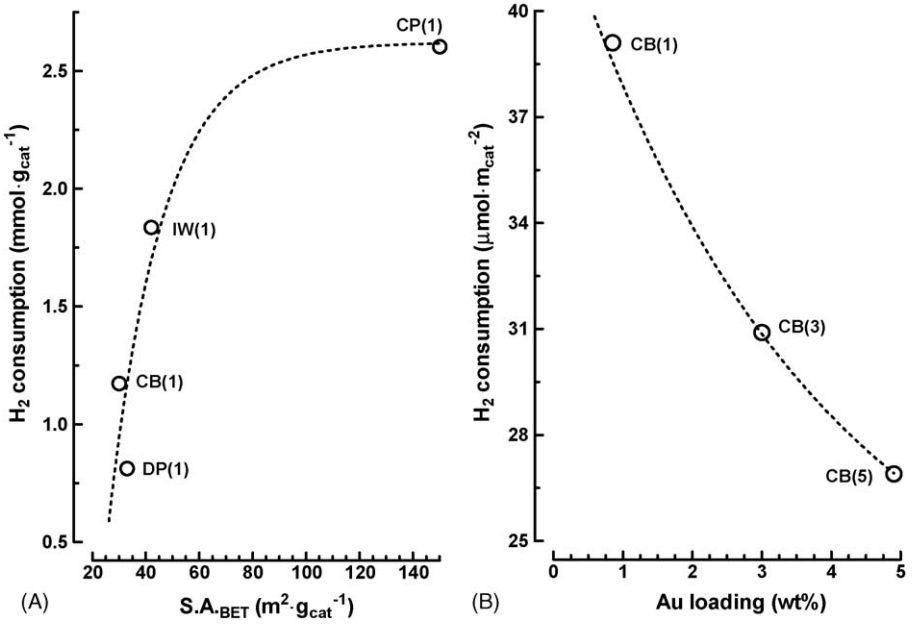

Fig. 3. Influence of surface area (A) and Au loading (B) on the total H_2 consumption of YY(1) and CB(x) catalysts, respectively.

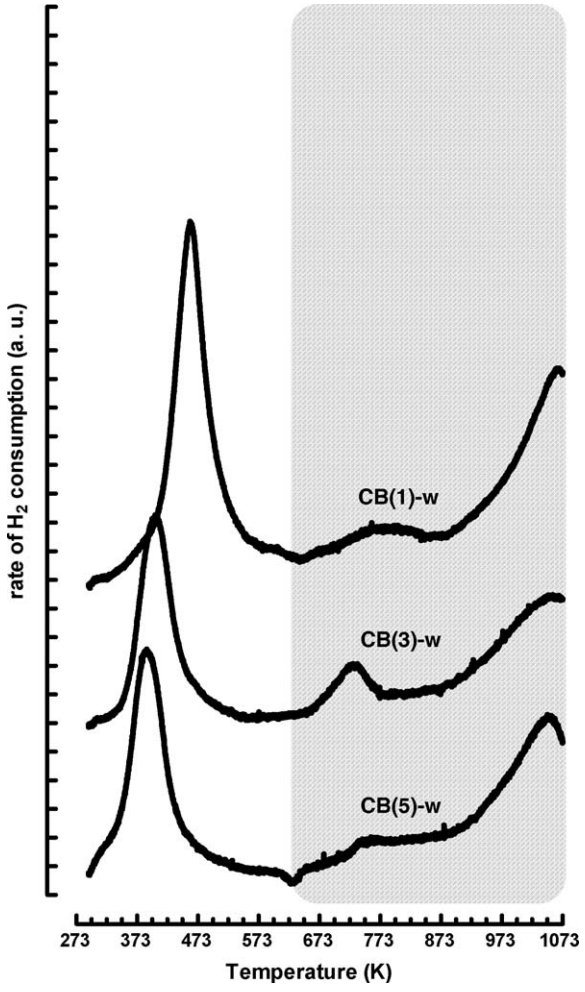

Fig. 4. TPR profiles of the CB(x)-w catalysts (the dashed grey area includes the temperature range for reduction of the ceria support).

tively, which control the extent of the catalyst reduction, as shown in Fig. 3.

The effects of chlorine elimination on the reduction pattern of the Au/CeO_2 system are observable from Fig. 4, comparing the TPR profiles of CB(x) and CB(x)-w catalysts. The characteristic temperatures and the extent of H_2 consumption are reported in Table 3. Chlorine removal improves greatly the reduction of the active phase, as all the CB(x)-w catalysts still display one peak, but characterised by a $T_{o,red}$ close to r.t. and a T_{M1} value of 390–460 K, which account for a negative shift of the former by ca. 100 K and of the latter by 40–80 K with

Table 3
TPR data of CB(x) catalysts (effect of the "washing" treatment)

Sample	$T_{o,red}$ (K)	T_{M1} (K)	T_{M2} (K)	H_2 consumption	
				μmol/g_{cat}[a]	H_2/Au[b]
CB(1)-w	300	460	1052	822	11.8
CB(3)-w	300	402	1052	801	1.9
CB(5)-w	296	390	1056	823	1.0

[a] In the range 273–1073 K.
[b] In the range 273–623 K.

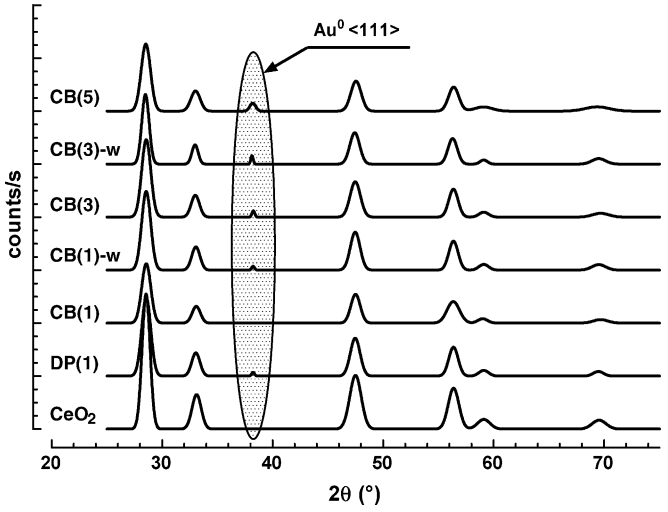

Fig. 5. XRD patterns of the CeO_2 support and Au/CeO_2 catalysts.

respect to the "untreated" samples (Table 2). Moreover, a lower peak intensity accounts for a H_2/Au ratio decreasing from 12.1 (CB(1)-w) to 1.0 (CB(5)-w).

4.2. Structural features

The XRD patterns of the ceria support, of the "untreated" and "washed" DP(1), CB(1), CB(3), CB(5) catalysts are shown in Fig. 5. All the spectra present the typical diffraction lines of the *cerianite* with the fluorite-like structure [21–24,29,32]. A slight reflex at 38.19°, typical of the Au ⟨1 1 1⟩ face [32], is observable in the XRD patterns of the DP(1), CB(1)-w, CB(3), CB(3)-w and CB(5) samples. From the line-width of the ⟨1 1 1⟩ reflexes of Au and ceria phases, the mean particle size values in Table 4 were calculated. The mean Au particle size varies between 7 nm (CB(5)) and 11 nm (DP(1)), being evident an appreciable growth further to the alkali washing treatment. According to the similar SA_{BET} values (Table 1), no significant differences (9–11 nm) in the ceria particle size are found.

Representative TEM pictures of the DP(1) (A), CB(1)-w (B) and CB(3)-w (C and D) at different magnifications are shown in Fig. 6. At lower magnification, all the samples appear as agglomerates of "small" (10–15 nm) ceria particles, where metal clusters with a size variable from few (<5 nm) to 10–15 nm are somewhat distinguishable. At higher magnification (Fig. 6D), (*quasi*)spherical Au particle(s) with a size diameter of 5–7 nm "embedded" in the ceria structure can be recognised on the CB(3)-w sample.

Table 4
XRD estimate of the average particle size of Au and ceria in the various catalysts

Sample	d_{Au} (nm)	d_{CeO_2} (nm)
CeO_2	–	11
DP(1)	11	11
CB(1)-w	8	10
CB(3)	8	9
CB(3)-w	9	10
CB(5)	7	10

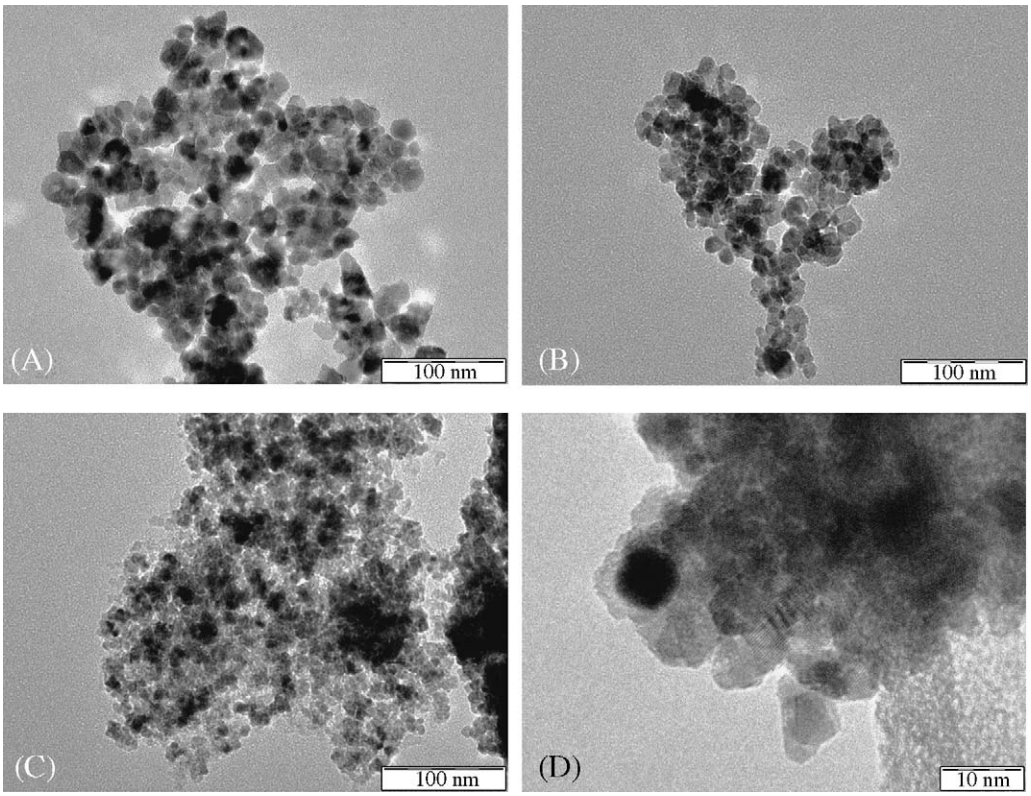

Fig. 6. TEM images of the (A) DP(1), (B) CB(1)-w and (C and D) CB(3)-w catalysts at different magnifications.

4.3. Total (TOX) and selective (PROX) CO oxidation pattern

Catalytic data in the TOX reaction of the ''untreated'' YY(1) samples, in terms of CO conversion with temperature (A) and Arrhenius plot (B), are shown in Fig. 7. Marked differences in both the onset temperature of CO oxidation ($T_{o,CO}$) and final (473 K) conversion values are evident spanning from DP to IW routes.

Namely, with the lowest $T_{o,CO}$ (300 K) and a conversion of ca. 60% at 473 K, the DP(1) catalyst results the most active system. The CP(1) is characterised by a rather high ignition

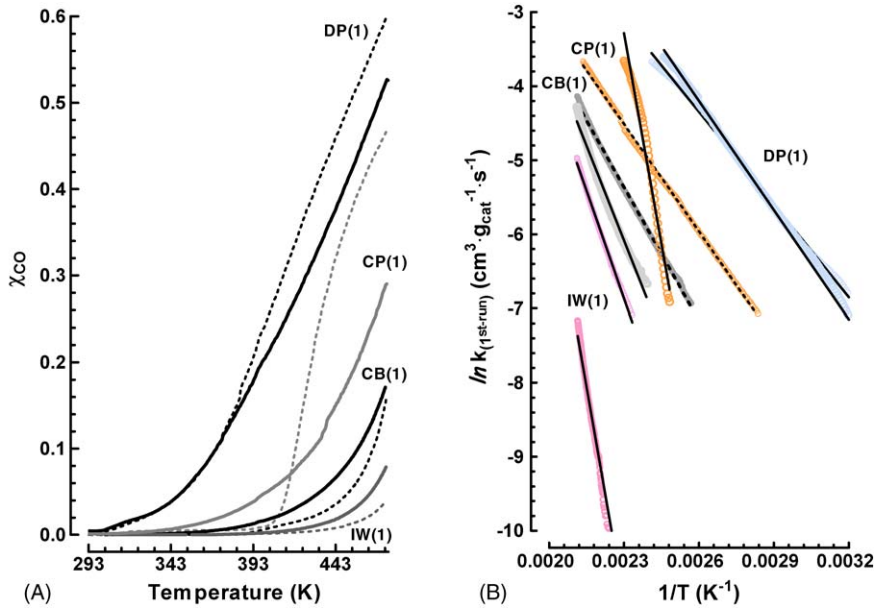

Fig. 7. TOX activity data of YY(1) catalysts in the 1st (dotted lines) and at ''stationary'' conditions (solid lines) in the range 273–473 K. (A) CO conversion vs. T and (B) Arrhenius plots.

Table 5
TOX activity data of the YY(1) catalysts

Catalyst	Temperature range (K)	r^2	E_{app} (kcal/mol)
1st reaction cycle			
DP(1)	313–409	0.994	10
CP(1)	403–435	0.970	38
CB(1)	428–473	0.979	27
IW(1)	435–474	0.990	39
Stationary activity			
DP(1)	314–416	0.998	10
CP(1)	352–470	0.998	10
CB(1)	389–470	0.999	12
IW(1)	428–474	0.997	19

Arrhenius plot data in the 1st reaction cycle and at ''stationary'' conditions (2nd–4th reaction cycles).

temperature ($T_{o,CO}$, 390 K), while the X_{CO} increases sharply to a value of ca. 45% at 473 K. The reactivity of the IW(1) and CB(1) systems is much lower as, in spite of $T_{o,CO}$ values comparable with that of the previous system, at 473 K they achieve X_{CO} values of only 4 and 7%, respectively. The Arrhenius plots (Fig. 7B) depict straight-line correlations ($r^2 > 0.970$), providing E_{app} values between 9 kcal/mol (DP(1)) and 39 kcal/mol (IW(1)), in a qualitative agreement with the activity scale of $T_{o,CO}$ and X_{CO} values.

To ascertain stationary activity levels, disregarding the influence of transient activation–deactivation phenomena, all the catalysts were subjected to four consecutive reaction cycles. After significant changes from the first (dotted lines) to the second cycle, the activity kept unchanged (within the experimental error) until the fourth run (solid lines). Then, stationary activity data (A) and relative Arrhenius plots (B) of the ''untreated'' YY(1) catalysts are compared in Fig. 7, the E_{app} values being included in Table 5. The DP(1) catalyst displays only a minor decrease in activity at $T > 373$ K, whilst for the

Table 6
TOX activity data of CB(x)-w catalysts

Catalyst	Temperature range (K)	r^2	E_{app} (kcal/mol)
CB(1)-w	345–394	0.999	10
CB(3)-w	319–392	0.999	11
CB(5)-w	321–358	0.990	13

Arrhenius plot data at ''stationary'' conditions.

CB(1) and IW(1) systems a downward shift of $T_{o,CO}$ (300 K) by ca. 100 K mirrors a much higher activity, leading to final X_{CO} value of ca. 15 and 8%, respectively. An analogous negative shift of $T_{o,CO}$ on the CP(1) catalyst (300 K) accounts for a remarkable rise in activity at $T < 400$ K and a decrease in the range 400–473 K, rendering more regular the rise of X_{CO} with T (Fig. 7A). Very accurate ($r^2 > 0.997$) Arrhenius plots (Fig. 7B) provide much lower E_{app} values (8–12 kcal/mol), with the exception of the IW(1) sample still characterised by the highest energetic barrier (19 kcal/mol). These data can be synthesised into the following activity scale for ''untreated'' catalysts:

$$DP > CP \gg CB > IW$$

The effect of chlorine removal on the catalytic performance was probed by comparing activity data at ''stationary'' conditions (2nd run) of the ''untreated'' CB(x) and ''washed'' CB(x)-w catalysts. The trends of X_{CO} with T (A) and the relative Arrhenius plot (B) are shown in Fig. 8, while the E_{app} values are summarised in Table 6. Removal of chlorine improves greatly the activity of any CB(x) catalysts, levelling off the TOX functionality with respect to the preparation method also in terms of E_{app} values (10–13 kcal/mol). The CB(1)-w catalyst (Fig. 8A) features in fact conversion levels comparable with those of the DP(1) sample (dotted line) while, reaching a full CO conversion at 445 K, the most active CB(5)-w system ensures specific activity values comprised between 0.02 and

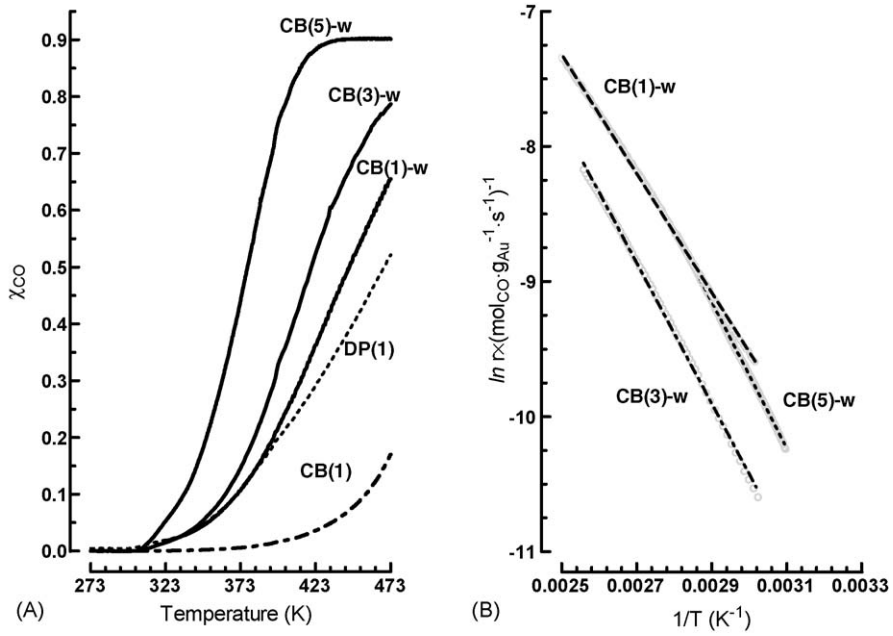

Fig. 8. TOX activity data of the CB(x)-w catalysts at ''stationary'' conditions. (A) CO conversion vs. T and (B) Arrhenius plots.

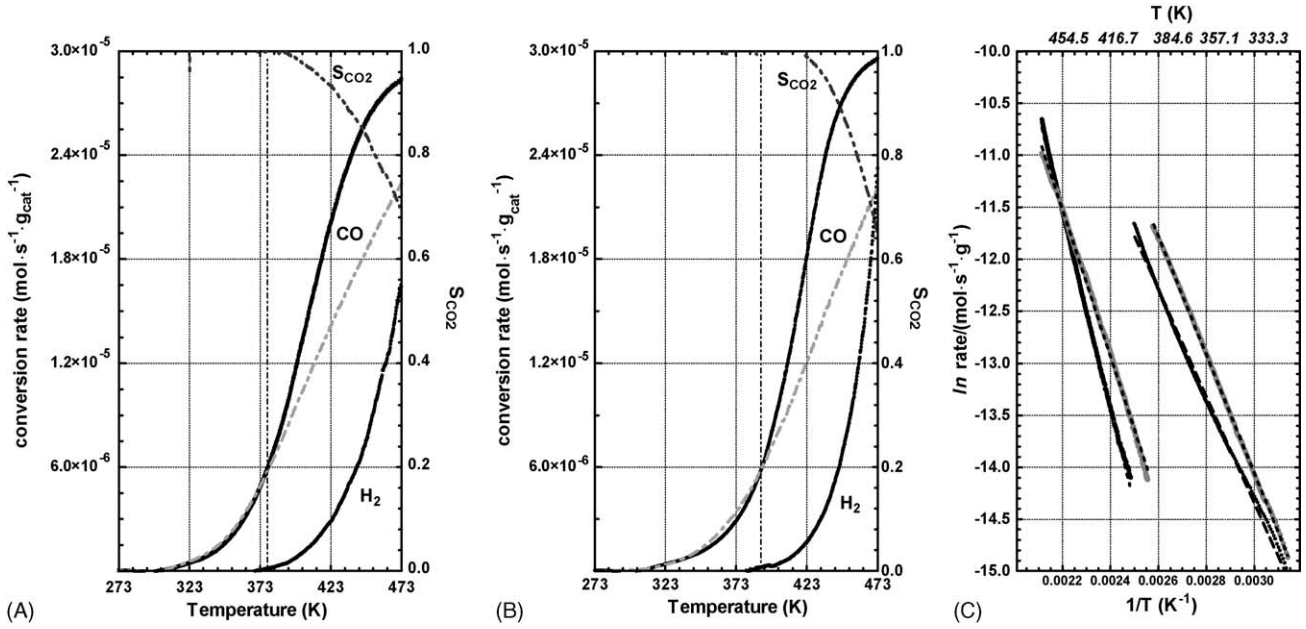

Fig. 9. PROX activity–selectivity data of the DP(1) (A) and CB(1)-w (B) catalysts at "stationary" conditions. (A and B) CO conversion vs. T and (C) Arrhenius plots of CO and H_2 conversion rates.

0.4 mol_{CO} $(mol_{Au}\ s)^{-1}$ in the range 273–440 K. On the whole, the TOX activity level parallels the Au loading (Fig. 8A), while the specific Au activity results the highest on the CB(1)-w and CB(5)-w catalysts (Fig. 8B).

The catalytic behaviour of DP(1) and CB(1)-w samples in the PROX reaction at "stationary" conditions is compared in Fig. 9 in terms of CO and H_2 conversion rate with T (A and B) and Arrhenius plots (C). Both catalysts display an analogous activity pattern resulting in a CO conversion practically unaffected by the presence of H_2 until a T of 380–400 K, below which no formation of water occurs (S_{CO_2}, 100%). Thereafter, an increasing rate of water formation parallels an enhanced CO conversion, resulting in a progressive S_{CO_2} decrease from 100 to ca. 65 and 75% at 473 K, respectively. In terms of activation energy (Table 7), these data mirror unchanged E_{app} values of CO oxidation (10–11 kcal/mol), while that of the H_2 oxidation is generally higher, going from 14 kcal/mol (DP(1)) to 19 kcal/mol (CB(1)-w), respectively.

5. Discussion

5.1. Structure and redox properties

It is generally recognised that *co-precipitation*, *deposition–precipitation* and *phosphine routes* confer a superior catalytic performance to supported-gold catalysts owing to an improved dispersion and complete absence of chlorine [4–7,10–20,26–28]. The inadequacy of conventional impregnation routes has been primarily associated with a low dispersion of the active phase caused by residual chlorine during thermal treatments [4–7,20,24,26,28]. However, a marked poisoning effect at Cl/Au ratios as low as 0.0006 on the selective CO oxidation activity of Au/Al_2O_3 catalysts led Oh et al. to argue a strong chemical effect of chlorine on a *small fraction of sites* having an *extremely high activity* [28].

Different synthesis routes, yielding substantial variations in residual chlorine (Cl_{at}/Au_{at}, 0–3.8) and total surface area (25–150 m^2/g), can be helpful for ascertaining the main factors affecting structure and reactivity of the Au/CeO_2 system.

A definitive assessment of metal dispersion and morphology is not straightforward since a statistical analysis of the particle size distribution by TEM observations is complicated by the peculiar structural features of the Au/CeO_2 system, hindering a definitive identification of very small sized Au clusters [22–24,27,29]. Although, an average size diameter of 7–11 nm, calculated from the XRD Au ⟨1 1 1⟩ reflex (Table 5), could realistically account for the metal dispersion of the various systems (Fig. 6), these values are well above the optimum range (2–3 nm) ensuring an effective catalytic functionality [2–7,10–20,24–28]. Nevertheless, the enhanced activity of the studied systems, which well compares with that of very active Au catalysts [4–7,10–18,25–29], suggests that dispersion would not be the only one parameter useful for rationalising the catalytic pattern, likely depending also on the morphology of metal particles [4–7,22,23].

The peculiar reactivity of ceria-supported systems, allows to get indirect information on dispersion of the active phase precursor from the synergetic effect on reduction of neighbouring Ce^{4+} ions [22,23,30]. The reduction of the ceria support in

Table 7
TOX and PROX activity data of the DP(1) and CB(1)-w catalysts

Catalyst	$E_{app,CO}$ (kcal/mol)	r^2	E_{app,H_2} (kcal/mol)	r^2
CB(1)-w	10	0.996	19	0.996
DP(1)	10	0.999	14	0.999

Arrhenius plot data at "stationary" conditions.

concomitance with that of the active phase will thus result in H_2/Au ratios (Table 2) larger than the stoichiometric value and it is expected to rise with dispersion of reducible Au^{3+} ions [23,30]. This explains the positive effect of surface area on catalysts reducibility (Fig. 3A) and the opposite decreasing trend of H_2 consumption with loading for the CB series (Fig. 3B). In other words, Fig. 3 proves that varying the preparation method or, for a same preparation method, the Au loading, the extent of hydrogen consumption would be fairly related to the dispersion of the Au precursor(s). Anyhow quite large H_2/Au ratios (Table 2) signal a strong promoting effect of Au ions on the reduction (or *spillover*) of ceria support [21–23,30]. Thus, a high Au^{3+} dispersion implies a strong enhancement of the catalyst reducibility but, as consequence of a strong interaction with the support, also a hard reduction of the active phase. As the high affinity of chloride for Au ions [28] and ceria lattice [30], this is particularly evident for CB(x) and IW(1) ''Cl-containing'' systems, even if TPR data signal that an effective, though weaker, ''Au^{3+}–CeO_2'' interaction occurs also in the CP(1) sample where, in spite of the absence of Cl, a quite high dispersion of Au^{3+} ions is expected as a consequence of a very large surface area [22–24,29]. At least, alkali washing treatment displaces chlorine from the catalyst, forming quite reducible Au^{3+} oxo-complexes [26–28], which easily give rise to metal particles as confirmed by both XRD spectra (Fig. 5) and TPR data (Fig. 4) of the CB(x)-w samples.

Therefore, the reduction patterns mirror different physico-chemical properties linked to the specificities of each preparation method, which can be rationalised as follows:

(a) DP(1) catalyst prepared using a ''pre-shaped'' support and ''free'' from residual chlorine (Cl_{at}/Au_{at}, 0);
(b) CP(1) catalyst obtained forming support and active phase into solution, ''free'' from residual chlorine (Cl_{at}/Au_{at}, 0);
(c) CB(x) catalysts prepared forming both support and active phase by reaction at high temperature (1200 K), and containing a fraction of residual chlorine (Cl_{at}/Au_{at}, 1.5–1.8);
(d) IW(1) catalyst prepared using a ''pre-shaped'' support and containing the ''undecomposed'' Au precursor ($Cl_{at}/Au_{at} \approx 4$).

DP (a) and IW (d), though involving a ''pre-shaped'' support of which they retain the main physical features (Table 1), lie at opposite ends with the lowest and largest amount of residual chlorine, which correspond to the easiest and hardest reduction, respectively. The combustion route (c) implies a partial decomposition of the Au precursor with the retention of a significant fraction of residual chlorine, which causes a consequent shift of both $T_{o,red}$ and T_{M1} upward by ca. 80 and 110 K with respect to DP. Favoured by the effect of the ultrasound irradiation [31], CP at basic pH (b) ensures the absence of chlorine along with a very high development of total surface area [31] which, enabling a ''molecular'' dispersion of the Au precursor across the ceria matrix, leads to a reduction intermediate between that of CB and DP catalysts. Similar structural features of the ''washed'' CB(x)-w samples explain a constant H_2 consumption (Table 3) irrespective of the loading evidently due to the ''saturation'' of the most defective position of the ceria surface able to ''accommodate'' Au^{3+} ions. Chlorine elimination, weakening the Au^{3+}–CeO_2 interaction, allows then for the appearance of the characteristic reduction peak of surface Ce^{4+} ions in the TPR spectra of the same systems (Fig. 4). Such findings are summarised in the structural models of Au/CeO_2 catalysts in Fig. 10, showing the coexistence of the following structures: (i) ''isolated'' Au^{3+} ions, with chlorine and/or oxo-ligands in the first coordination shell; (ii) ''bulk'' metal clusters and (iii) $Au^{\delta+}$ ions at the Au^0/CeO_2 interface.

5.2. Catalytic behaviour in TOX and PROX reactions

In spite of the presence of Au particles on the ''untreated'' CB(3) and CB(5) samples (Fig. 5), the downward shift of $T_{o,CO}$ and the consequently higher TOX activity recorded for the CB(x) and CP(1) catalysts at stationary conditions (Fig. 7), signal that a small amount of *active* sites is generated by reduction of Au^{3+} ions during the 1st reaction cycle. The decisive role of the Au precursor reduction during the 1st reaction cycle is definitively proved by direct relationships amongst $T_{o,red}$ (Table 2), $T_{o,CO}$ and E_{app}, shown in Fig. 11. In

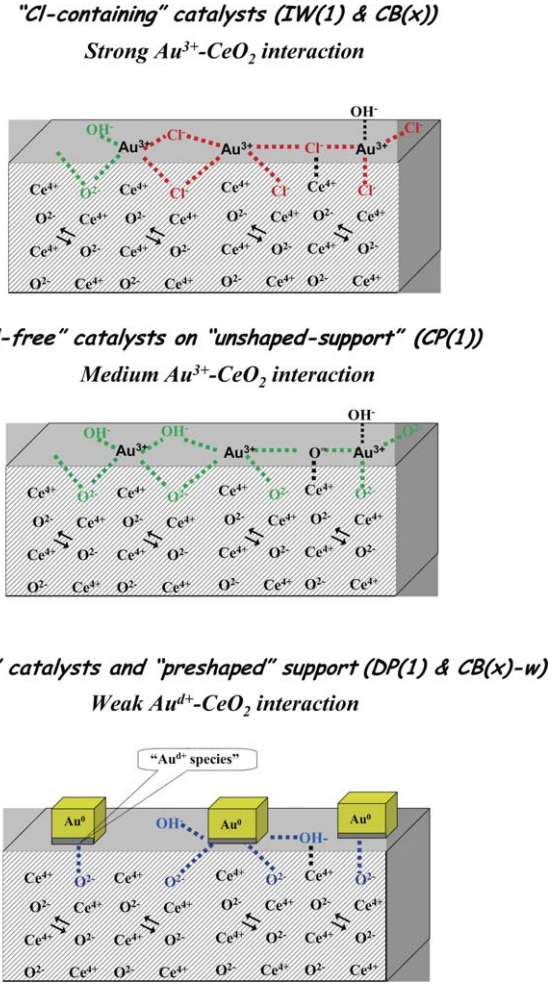

Fig. 10. Structural models of Au/CeO_2 catalysts.

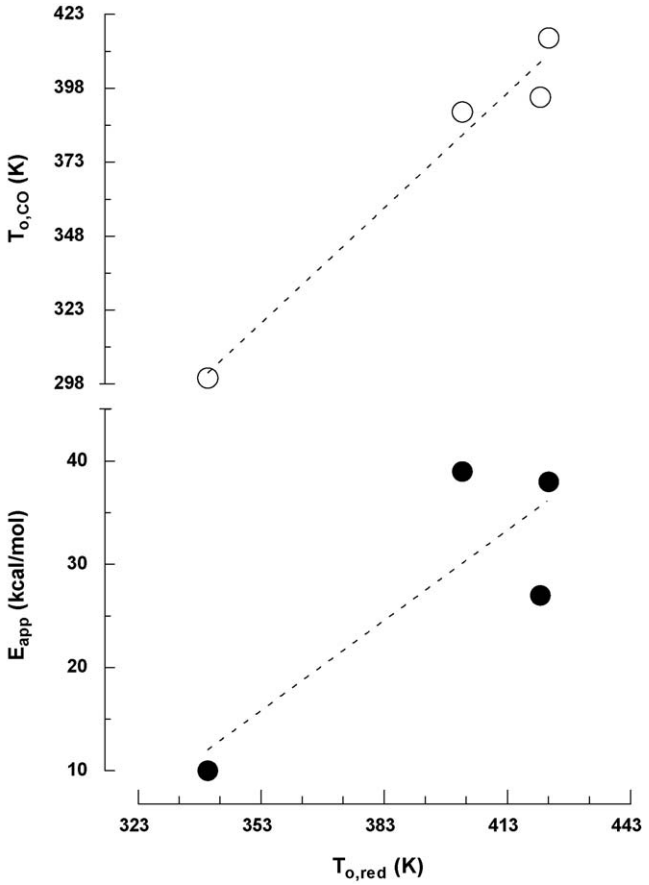

Fig. 11. Relationships amongst $T_{o,red}$, $T_{o,CO}$ and E_{app} values of the "untreated" YY(1) catalysts in the 1st reaction cycle.

particular, the increasing relationship between $T_{o,red}$ and E_{app} would match the fact that the r.d.s. of the CO oxidation on "untreated" catalysts is the "abstraction" of the catalyst oxygen for generating (partially) reduced $Au^{\delta+}$ species [2–7]. This reflects on very high values of the energetic barrier (27–39 kcal/mol), well above the 9 kcal/mol value of the easily reducible DP(1) sample. A high "mobility" of lattice oxygen coming from the simultaneous reduction of the ceria support (Fig. 1), accounts for the abrupt rise of CO conversion at $T > 400$ K on the "untreated" CP(1) catalyst (Fig. 7). On the other hand, matching the value (25.5 kcal/mol) found by Bera and Hegdè for an analogous catalyst, the value of 27 kcal/mol of the CB(1) sample seems to be fairly related to residual chlorine rather than to a poor metal dispersion [21]. Therefore, the reduction of strongly interacting Au^{3+} ions during the 1st reaction cycle generates active sites, reflecting in a substantial decrease of the energetic barrier (8–12 kcal/mol) at "stationary" conditions, consistently with literature data for supported Au systems [2–7,28]. However, the presence of chlorine still hinders an effective catalytic activity due to the strongly "poisoning" effect on active sites [26–28]. Chlorine elimination, then, determines a further marked improvement of the stationary activity of CB(x)-w catalysts, *levelling off* any residual difference linked to the preparation method [28]. The different activity of the CB(x)-w catalysts (Fig. 8) could be then related to different populations of active sites in the various systems and, though specific gold activity data (Fig. 8B) match with a similar higher dispersion of CB(1)-w and CB(5)-w samples, the slight differences in the mean particle size estimate (Table 5) could not fully explain the observed differences in activity.

The analogous activity–selectivity pattern of the DP(1) and CB(1)-w catalysts in the PROX reaction (Fig. 9) confirms the decisive role of residual chlorine on the performance of supported Au catalysts [4–7,26–28]. According to Carrettin et al. who experienced a total carbon dioxide selectivity on a "microcrystalline" ceria-supported Au catalyst in the PROX reaction [29], both the DP(1) and CB(1)-w samples drive rather selectively the CO oxidation up to ca. 380 K, keeping the same activity level recorded in TOX tests (grey dotted lines). Thereafter, with starting the oxidation of H_2, the rate of CO conversion increases more than in total oxidation, probably as a consequence of the establishing of a parallel WGS reaction path, driven effectively by Au/CeO_2 catalysts [22–24]. Not consistent with the CO conversion decrease observed at 333 K by Carrettin et al. [29], this could be due to a diverse reactivity of the ceria support, likely affecting the adsorption pattern of reactant and product species. Indeed, even if a higher energetic barrier of the hydrogen oxidation (Table 7) matches in any case with a major affinity of the Au catalysts for CO rather than for H_2 adsorption [2–7], the different E_{app} value recorded for the DP(1) (14 kcal/mol) and CB(1)-w (19 kcal/mol) catalysts suggests that the morphology of both the active phase and ceria support plays a decisive influence on the reactivity of the Au/CeO_2 catalyst in the PROX reaction [29].

6. Conclusions

- The preparation method controls the strength of the Au^{3+}–CeO_2 interaction by determining both the amount of residual chlorine and total surface area.
- Hindering the reduction of the active phase, residual chlorine plays a strong poisoning effect on the catalytic activity of the Au/CeO_2 system.
- Dispersion is not the only one parameter determining the reactivity of the Au/CeO_2 catalyst.
- Removal of residual chlorine by washing treatments in alkali solutions enhances the reducibility of the active phase, *levelling off* the functionality of the Au/CeO_2 system in both TOX and PROX reactions.
- The Au/CeO_2 system drives selectively the CO oxidation in presence of hydrogen up to 373 K deserving potential application for low-temperature fuel cells devices.

References

[1] B. Hammer, J.K. Norskov, Nature 376 (1995) 238.
[2] M. Haruta, Catal. Today 36 (1997) 153.
[3] M. Haruta, M. Daté, Appl. Catal. A 222 (2001) 427.
[4] M. Haruta, CATTECH 6 (2002) 102.
[5] A.I. Kozlov, A.P. Kozlova, H. Liu, Y. Iwasawa, Appl. Catal. A 182 (1999) 9.
[6] G.C. Bond, D.T. Thompson, Gold Bull. 33 (2000) 41.
[7] G.C. Bond, D.T. Thompson, Catal. Rev.-Sci. Eng. 41 (1999) 319.
[8] D.T. Thompson, Appl. Catal. A 243 (2003) 201.

[9] R. Meyer, C. Lemire, Sh.K. Shaikhutdinov, H.-J. Freund, Gold Bull. 37 (2004) 72.
[10] A. Ueda, M. Haruta, Gold Bull. 32 (1999) 3.
[11] T. Hayashi, K. Tanaka, M. Haruta, J. Catal. 178 (1998) 566.
[12] G. Mul, A. Zwijnenburg, B. Van der Linden, M. Makkee, J.A. Moulijin, J. Catal. 201 (2001) 128.
[13] B. Nkosi, M.D. Adams, N.J. Coville, G.J. Hutchings, J. Catal. 128 (1991) 378.
[14] G. Hutchings, Catal. Today 72 (2002) 11.
[15] M. Haruta, N. Yamada, T. Kobayashi, S. Iijima, J. Catal. 115 (1989) 301.
[16] M. Haruta, S. Tsubota, T. Kobayashi, H. Kageyama, M.J. Genet, B. Delmon, J. Catal. 144 (1993) 175.
[17] D.W. Goodman, M. Valden, X. Lai, Science 281 (1998) 1647.
[18] G.R. Bamwenda, S. Tiubota, T. Nakamura, M. Haruta, Catal. Lett. 44 (1997) 83.
[19] M.M. Schubert, S. Hackenberg, A.C. van Veen, M. Muhler, V. Plzak, R.J. Behm, J. Catal. 197 (2001) 113.
[20] A. Wolf, F. Schüth, Appl. Catal. A 226 (2002) 1.
[21] P. Bera, M.S. Hegdé, Catal. Lett. 79 (2002) 75.
[22] Q. Fu, A. Weber, M. Flytzani-Stephanopoulos, Catal. Lett. 77 (2001) 87.
[23] Q. Fu, S. Kudriavtseva, H. Saltsburg, M. Flytzani-Stephanopoulos, Chem. Eng. J. 93 (2003) 41.
[24] T. Tabakova, F. Boccuzzi, M. Manzoli, J.W. Sobczak, V. Idakiev, D. Andreeva, Appl. Catal. B: Environ. 49 (2004) 73.
[25] S.D. Lin, M. Bollinger, M.A. Vannice, Catal. Lett. 17 (1993) 245.
[26] J.M.C. Soares, P. Morral, A. Crossley, P. Harris, M. Bowker, J. Catal. 219 (2003) 17.
[27] R.J.H. Grisel, B.E. Nieuwenhuys, J. Catal. 199 (2001) 48.
[28] H.-S. Oh, J.H. Yang, C.K. Costello, Y.M. Wang, S.R. Bare, H.H. Kung, M.C. Kung, J. Catal. 210 (2002) 375.
[29] S. Carrettin, P. Concepción, A. Corma, J.M. López Nieto, V.F. Puntes, Angew. Chem. Int. Ed. 43 (2004) 2538.
[30] A. Trovarelli, Catalysis by Ceria and Related Materials, Imperial College Press, London, 2002.
[31] N. Arul Dhas, A. Ekhtiarzadeh, K.S. Suslick, J. Am. Chem. Soc. 123 (2001) 8310.
[32] Joint Committee Powder Diffraction System, International Centre for Diffraction Data, Swarthmore (USA).